Fuel 345 (2023) 128161

Contents lists available at ScienceDirect

Fuel

journal homepage: www.elsevier.com/locate/fuel

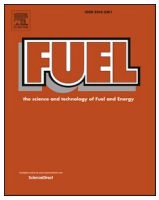

Full Length Article

Influence of the radial-lip concept design to achieve ultra-low soot emission reductions: An optical analysis

José V. Pastor [a], Carlos Micó [a,*], Felipe Lewiski [a], Francisco J. Tejada [a], Alberto Vassallo [b], Francesco C. Pesce [b], Giacomo Belgiorno [b]

[a] CMT – Motores Térmicos, Universitat Politècnica de València, Camino de Vera s/n, 46022, Spain
[b] PUNCH Torino S.p.A, Corso Castelfidardo, 36, 10129 Torino, TO, Italy

ARTICLE INFO

Keywords:
Compression ignition
Optical engine
Soot formation
Radial lips
Piston geometry
Emission reduction

ABSTRACT

Nowadays, internal combustion engines must reduce pollutant emissions to achieve the upcoming strict regulations in the transport sector. In this context, new hardware designs have shown great potential to reduce pollutant emissions and comply with current and future regulations. This paper focuses on innovative bowl designs with radial lip protrusions, which are radially distributed inside the bowl. The potential of using these protrusions in order to reduce soot formation and improve soot oxidation has been demonstrated by different studies. For this reason, the present work addresses the impact of using two different radial-lip based geometries on soot formation and combustion behaviour in an optical single-cylinder compression ignition engine. High-speed OH* chemiluminescence imaging and 2-Colour pyrometry were applied simultaneously, in combination with a thermodynamic analysis of the in-cylinder pressure signal. The results show that more pronounced radial-lip geometry drive the flames closer to the bowl centre, where more oxygen is available to oxidize the soot, resulting in in-cylinder soot formation reduction. In addition, it has been observed that the improvement achieved by the more pronounced radial-lip geometry is more noticeable under high EGR conditions. This opens a path to reduce the soot-NO_X trade-off in compression ignition engines.

1. Introduction

The reduction of pollutant emissions in the transport sector, especially from internal combustion engines (ICE), is necessary to achieve the strict emission regulations imposed by governments. Emissions from transport account for one quarter of the European Union (EU) greenhouse gas (GHG) emissions. The EU domestic transport emissions increased by 0.8% between 2018 and 2019, from which road transport represents the highest contribution. In 2019, it produced 72% of all domestic and international transport GHG [1]. In addition, soot and nitrogen oxides (NO_X) are the most deadly and critical atmosphere pollutants. Heavy-duty diesel vehicles contribute to 80% of transport-related emissions of these species [2]. Despite great efforts have been put into their mitigation, the well-known soot and NO_x trade-off makes it difficult to reduce one of them without increasing the other. These facts have motivated the industry and researchers to look for alternatives to reduce, as much as possible, the pollutant emissions. Electrification in vehicles as a powertrain has shown to be very promising for light-duty vehicles. However, in medium and heavy-duty applications, it is still a big challenge and in the short and medium-term internal combustion engines (especially compression ignition engines) will still play an important role in the transport sector. Therefore, the search of new alternatives to reduce the environmental impact of the ICE technology are a key point to comply with emission regulations while a transition to different solutions is achieved.

With this objective, researchers have been working on different strategies. One of the main trends in the last decade has been the development of alternative combustion strategies, such as the Reactivity

Abbreviations: EU, European Union; GHG, Greenhouse gas; ICE, Internal combustion engine; CI, Compression ignition; CDS, Controlled diffusive spray; STD, Standard injector; OH*, Excited state hydroxyl radical; 2C, 2-Colour pyrometry; CS1, Combustion system 1; CS2, Combustion system 2; CAD, Crank angle degree; aHRR, Apparent heat release rate; IMEP, Indicated mean effective pressure; P_{int}, Intake pressure; P_{exh}, Exhaust pressure; T_{int}, Intake temperature; P_{inj}, Injection pressure; SOE, Start of energizing; % O_2, Oxygen concentration (volume); EGR, Exhaust gas recirculation; FWHM, Full width half maximum; KL, Soot optical thickness; aTDC, After top dead center.

* Corresponding author.
E-mail address: carmirec@mot.upv.es (C. Micó).

https://doi.org/10.1016/j.fuel.2023.128161
Received 13 December 2022; Received in revised form 27 February 2023; Accepted 17 March 2023
Available online 23 March 2023

Controlled Compression Ignition (RCCI) and the Partially Premixed Combustion (PPC) concepts [3–6]. The use of alternative fuels, such as biofuel and e-fuels [7,8], represents also an interesting path to reduce the GHG footprint and pollutant emissions, as well as reducing the dependence on fossil fuels.

Another path that has been traditionally exploited to achieve a cleaner and more efficient combustion is the new hardware design implementation. In a direct injection ICE (governed by diffusion combustion), in-cylinder soot formation and oxidation processes are directly related to the air/fuel mixture process [9,10]. It is mainly governed by the injection system (and injection strategy), in-cylinder thermodynamic conditions, fuel properties and piston geometry. However, a better air/fuel mixture implies an increase of energy release and flame temperature, which significantly enhances the NO_X formation. To avoid this, the focus can be put on the improvement of the oxidation process during the final stages of combustion [11]. For this purpose, piston geometry can play a major role due to the flame - bowl wall interaction as well as the swirl and squish flow dynamics. A proposal that can be found in literature is to implement bowl geometries that are able to redirect the flames towards areas of the piston where there is still oxygen available for the later oxidation of soot and unburned hydrocarbons [10]. For example, in compression ignition engines (CI), the re-entrant bowl design is typically used (blue line in Fig. 1). This design is named so because it re-direct the flames towards the piston centre after they impinge its walls. This promotes the consumption of oxygen still available in this region during the late stages of combustion and increases late soot oxidation [12]. The inclusion of a stepped lip at the upper part in the re-entrant bowl design could be considered an evolution (green line in Fig. 1), in comparison to the protruding lip of more conventional re-entrant bowl designs. The purpose of this feature is to split the sprays, driving part of the fuel towards the squish region to improve oxygen usage there. This concept has been implemented by different research groups [13,14]. The results of using new piston designs showed a significant reduction in soot emissions, as well as a shorter combustion duration that lead to thermal efficiency improvements and fuel consumption reductions, reducing CO_2 emissions [14–17]. Blasio et al tested a piston that included both radial and step lip geometries in a light-duty diesel engine. They found a reduction of up to 66% of the soot emission in comparison with a conventional reentrant piston. Regarding thermal efficiency improvements, Busch et al, reported an increase of 1.5% using a stepped bowl instead of the conventional one.

One of the most innovative recent bowl design proposals is the introduction of protrusions or radial lips at the periphery of a re-entrant bowl. It was originally presented by Volvo Group for heavy-duty engines and has been optimized by other companies. Up to 80% of soot emission reductions [18], as well as efficiency improvement [12] were reported. Some studies evaluated the combination of this new concept with the addition of a stepped lip at the top of the bowl for light-duty vehicles, with higher swirl ratios [9,19–21] (red line in Fig. 1). The results confirmed an improvement in mixture formation leading to in-cylinder soot formation reduction. However, this proposal can be still considered recent and not many works can be found in the literature that analyse the key aspects of its geometry and its relationship with the performance of the concept on different engine platforms and operating conditions.

The interaction of the bowl design with other elements, like the injector, are important for the final performance of the geometry utilized. Among different innovative injector concepts that can be found in literature, the CDS nozzle design (Controlled Diffusive Spray) has been proposed by different groups. It promotes the fuel combustion away from the bowl walls by producing shorter spray penetration and wider spray cone angle [22,23]. However, to the author's knowledge, not many works can be found in literature which this novel injection systems have been combined with the new bowl design proposals described in the previous paragraphs.

Considering all the above mentioned, the main objective of this study is to analyse the effect of different piston geometries, based on the radial-lip and stepped-lip proposals, on soot formation in an optical engine. On one hand, the use of the proposed innovative combustion system fills a gap found in literature about the use of these new concepts in these types of engine architectures and operating conditions. On the other hand, the comparison of different geometry proposals based on the same concepts allows for improving the understanding of the key aspects related to its performance. To achieve this, two different pistons were studied: a hybrid geometry and a symmetrical geometry. The first one presents radial lips only in one half of the bowl, combined with a stepped-lip feature at the edge of the re-entrant bowl. In this way, the effect of including or not the radial lips can be analysed simultaneously. The second one presents a geometry where radial lips are distributed all around the periphery of the bowl, which also presents a re-entrant geometry with a stepped-lip at the edge. The design of the radial-lips for each piston is different. In this way, the effect of its modification can be analysed.

The study has been performed under different operating conditions, which are propitious to high soot formation, in a single-cylinder optical engine (~0.8 L per cylinder). Besides, two different nozzle designs have been included (conical and CDS design). High-speed 2-Colour pyrometry and excited-state hydroxyl radical (OH*) chemiluminescence were used in this study with the aim of analysing the whole combustion process. Results highlight clear differences in the flame propagation when comparing the two different radial-lip geometries. The radial lips from the hybrid piston drive the flame closer to its centre where fresh oxygen is available. Furthermore, with high EGR conditions, the difference between the proposed radial-lip geometries becomes more apparent. The results suggest that the benefits of the hybrid piston radial-lip design take better advantage when oxygen concentration is low. This reinforces the idea that this new geometry proposal could provide great improvements on the mitigation of the soot-NO_X trade-off.

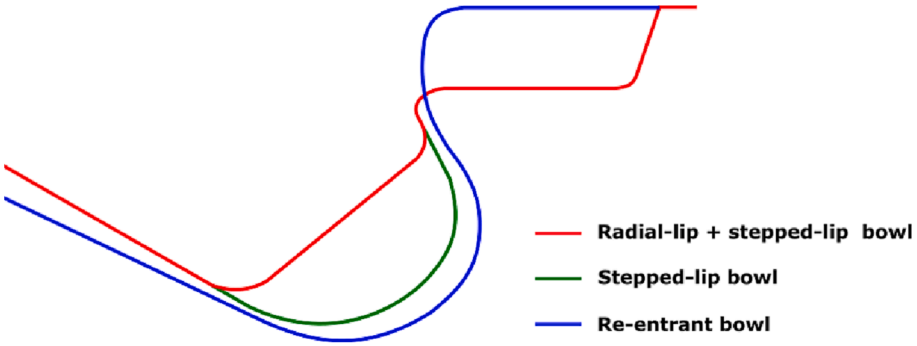

Fig. 1. Sketch of different bowl designs. Redrawn with permission from [10].

2. Experimental methodology

2.1. Optical engine

The experimental facility consists of a single-cylinder optical CI engine (Fig. 2). It is an overhead valve (OHV) type, where the valves are in the cylinder head (2 exhaust and 2 intake valves). A specific case, placed between the engine block and cylinder head to accommodate the camshaft and pushrods. In this way, this system replicates the original pushrod mechanism and keeps proper lubrication of the camshaft. The optical access is achieved through the base of the piston, thanks to an elliptical mirror located at 45° within a piston extensor. However, this engine was built with no lateral accesses, in contrast with most of the optical engines that can be found in the literature. The main advantage is that it allows utilizing a piston design where the rings are located closer to its top face, achieving a higher effective compression ratio than other facilities. The main characteristics are summarized in Table 1.

The engine was motored by an electric dynamometer. A screw compressor provided the intake air at the required pressure while a valve located at the exhaust pipe was used to simulate a backpressure of 0.2 bar over the intake one. Additionally, the required intake air temperature was ensured by an air heater located just before the intake port. Instantaneous intake and exhaust pressures were measured with a piezoresistive transducer (Kistler-4049A5). The in-cylinder pressure was obtained by using a piezoelectric transducer (Kistler-6124A). An oscilloscope (Yokogawa DL708E) was used for recording the pressure signal, which was synchronized with a crankshaft encoder with 0.5 CAD resolution. The apparent Heat Release Rate (aHRR) was calculated by applying a standard first-law thermodynamic analysis [24] by using the measured in-cylinder pressure. The engine was operated under skip-fire mode to minimize thermal stress and window fouling while avoiding any effect caused by thermal transients. Therefore, injection and combustion took place only one cycle every 20 motored cycles.

A conventional high-pressure pump (Bosch CP3) and common rail were used to deliver the fuel to the injector. In this study, two different nozzles were utilized: a standard 8-hole conical nozzle (STD); and a Controlled Diffusive Spray (CDS) 8-hole nozzle. An example of both designs can be observed in Fig. 3. The concept of the CDS nozzle aims to enhance the flexibility of distributing the spray in the combustion chamber. A shorter spray penetration and wider spray cone angle are achieved resulting in a combustion reaction closer to the centre of the

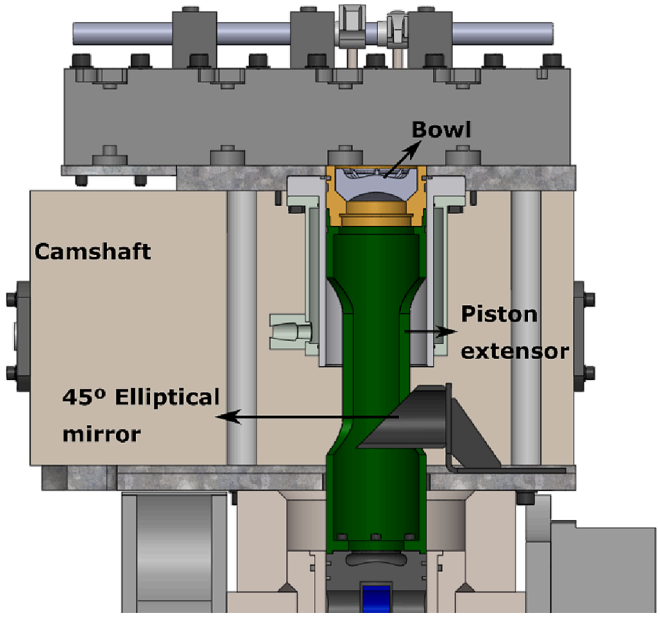

Fig. 2. Optical engine parts.

Table 1
Optical single cylinder engine characteristics.

Operational mode	Diesel engine
Number of cylinders [-]	1
Number of valves [-]	4
Bore/Stroke	~ 1
Displacement [L]	~ 0.8
Effective compression ratio	13.3

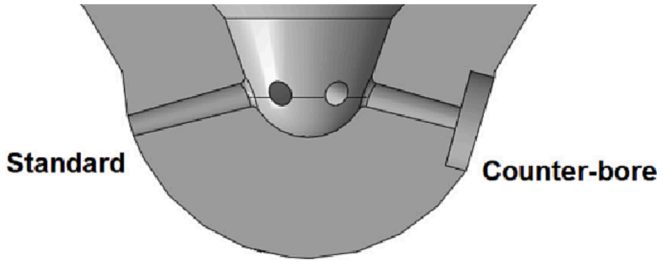

Fig. 3. Comparison of standard (left) and counter-bore (right) nozzle orifices. Reprinted with permission [22].

piston bowl rather than at the walls of the bowl, as it would be with a more conventional nozzle (STD) [25]. The CDS effect is achieved through counter-boring the holes of the nozzle. Numerical [26] and experimental [22,23] studies comparing STD and counter-bore nozzles among others can be found in the literature. Payri et al. [22] reported an appreciable decrease in pollutant emissions, especially in terms of particulate matter and hydrocarbon emissions due to the improvement of fuel–air mixing promoted by the counter-bore nozzle geometry.

The fuel used in this study is conventional diesel (biofree). Some interesting physical–chemical properties are summarized in Table 2.

Two different bowl designs were used in this study, which are shown in Fig. 4. From now on, they will be referred to as combustion system 1 (CS1) and combustion system 2 (CS2), corresponding to the left and right sketches, respectively. Both combine a stepped lip and radial lips. However, the geometry of CS2 presents several changes related to the radial lip and the bowl design, compared to CS1. These modifications were proposed to increase the influence of the new geometry over the air/fuel mixture process while not penalizing other aspects like thermal efficiency [17,20]. In addition, it was decided to build CS2 asymmetrical, with radial lips only in one sector of the circumference. The aim was to be able to isolate the effect of the re-designed radial lips from other additional modifications included in CS2 by comparing both halves of this piston. In Fig. 4, the blue shadowed area shows the region of the bowl with radial lips which was considered in the analysis (CS2-Lips).

2.2. Operating conditions

In this study, the influence of different operating conditions on both pistons' performance was evaluated. A set of baseline experimental conditions were defined (Table 3) corresponding to an operating point of 6.5 bar indicated mean effective pressure (IMEP). In addition, the oxygen concentration (% O_2) was reduced to 18% and 15% respectively to

Table 2
Fuel properties.

Parameter	Diesel
Density @15 °C (kg/m^3)	829.2
Viscosity @40 °C [mm^2/s]	2.59
Cetane number [-]	52.0
Oxygen content [%]	0
Lower heating value (MJ/kg)	41.92

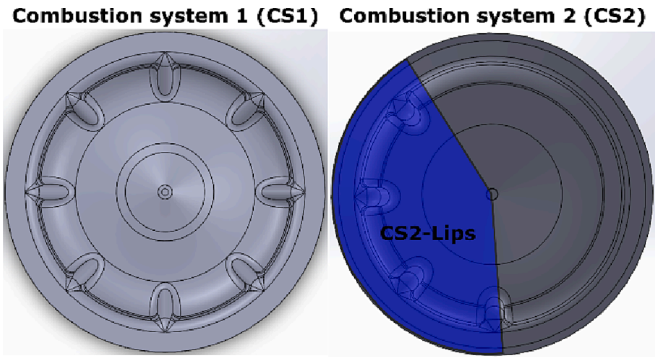

Fig. 4. Combustion system designs.

simulate exhaust gas recirculation (EGR). This reduction was achieved by diluting the airflow at the intake port with nitrogen (N_2). To avoid the influence of cycle-to-cycle variability on the analysis, 10 combustion cycles were registered per operating condition and data was averaged.

A realistic injection strategy was used including two pilot injections, one main injection and one post-injection. The dwell time between consecutive pulses and the duration of each pulse is presented in Fig. 5.

2.3. Optical techniques

Two optical techniques, 2-colour pyrometry and OH* chemiluminescence high-speed imaging, were applied simultaneously in order to analyse the soot formation and the oxidation process during combustion. The optical setup is shown in Fig. 6. With this setup, flame radiation goes through the quartz piston bowl and gets reflected by the 45° elliptical mirror (see Fig. 2). This element has an enhanced aluminium coating to obtain a good reflection efficiency in the UV and visible spectrum (above 85% between 250 and 700 nm). Then, radiation reaches a dichroic mirror (DMSP805L) that transmits the visible spectrum and reflects UV radiation in a small range of around 310 nm, coinciding with one of the most intense emission bands of the OH* radical. A high-speed camera equipped with a high-speed intensifier and a narrowband interference filter is used to register it. At the same time, the light transmitted through the dichroic mirror reaches a beam splitter that reflects 50% of it and transmits the other 50%. All this radiation is directed towards two high-speed cameras, equipped with specific narrowband interference filters to register only specific wavelengths, which is required to apply the 2-Colour pyrometry algorithm. The three high-speed cameras were triggered simultaneously with the SOE and synchronized on a frame basis. Thus, the image-by-image correlation between them was ensured.

2.3.1. OH* chemiluminescence imaging

A good tracer of high-temperature reactions in hydrocarbon diffusion combustion is the OH* chemiluminescence [27]. For this reason, high-speed OH* chemiluminescence images were used in this work to trace the oxidation reactions within the piston bowl. It is important to remark that the signal obtained was line-of-sight integrated, which limits the spatial resolution of the results.

For this technique, a Photron SA5 (high-speed CMOS) equipped with a Hamamatsu C10880-03F high-speed intensifier was used. The photocathode of the intensifier is a multialkali (S-20), which allows detection from UV to near IR (spectral response: 185–900 nm). The intensifier was coupled to the camera with 1:1 relay optics. An UV-Nikor Rayfact 105 mm f 4.5 was used as the system lens. A narrowband interference filter with central wavelength at 310 nm and 10 nm full width half maximum (FWHM) was set in front of the camera lens to register only the radiation corresponding to the OH* emission peak and reject the rest. The gating of the intensifier was the same as the exposure time of the high-speed camera, which was set at 39.75 μs. The intensifier gain was set at 38% for all tests. The acquisition speed was 25,000 frames per second (fps) and the resolution was 4.4 pixels/mm.

2.3.2. 2-Colour pyrometry

To apply the 2-Colour pyrometry technique, thermal radiation from soot at two different wavelengths is registered to determine the soot surface temperature. Knowing that the emissivity of a non-black body (ε_λ) can be defined by (1)

$$\varepsilon_\lambda = \frac{e^{\left(C_2/\lambda T\right)} - 1}{e^{\left(C_2/\lambda T_a\right)} - 1} \tag{1}$$

Where C_2 is the second Planck's constant, T is the real temperature, λ is the radiation wavelength and T_a is the apparent temperature (or brightness temperature). This last term can be defined as the temperature of a blackbody that will emit the same radiation intensity as a non-blackbody at temperature T with an emissivity of ε_λ.

In practice, the emissivity can be estimated for soot particles using the empirical correlation developed by Hottel and Broughton, as described in Eq. (2)

$$\varepsilon_\lambda = 1 - e^{-\left(KL/\lambda^\alpha\right)} \tag{2}$$

where K is an absorption coefficient that is proportional to the number density of soot particles and L is the geometric thickness of the flame along the optical axis of the detection system. The parameter α depends on the physical and optical properties of soot. Matsui et al. [28] studied the validation of the above correlation by simultaneous measurements of the soot emissivity at three different wavelengths in a diesel engine concluding that at least in the visible range this is a correct functional relation between emissivity and wavelength. Zhao et al. [29] reported that for the visible wavelength range, $\alpha = 1.39$ can be used for most fuels.

From Eqs. (1) and (2), the KL parameter can be obtained as represented in (3).

$$KL = -\lambda^\alpha \ln\left[1 - \left(\frac{e^{\left(C_2/\lambda T\right)} - 1}{e^{\left(C_2/\lambda T_a\right)} - 1}\right)\right] \tag{3}$$

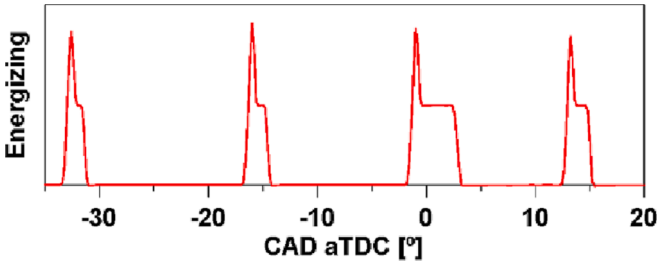

Fig. 5. Injection strategy.

Table 3
Baseline operating conditions.

Inj. Pattern	Engine Speed (rpm)	P_{int} (bar)	P_{exh} (bar)	T_{int} (°C)	P_{inj} (bar)	IMEP (bar)	SOE (° aTDC)	% O_2 (% vol.)
Multiple	1400	1.34	1.54	55.4	1182	6.7	–33.7	21

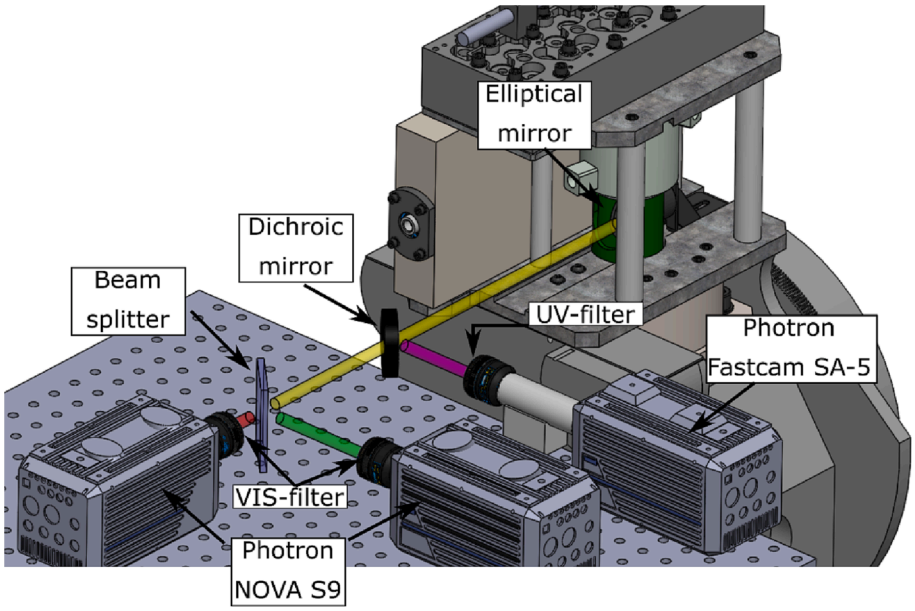

Fig. 6. Optical setup.

Assuming that the KL parameter does not vary with the change of the wavelength, as long as it belongs to the visible range and the alpha parameter does not change, (3) can be written for the two registered wavelengths λ_1 and λ_2 in order to obtain the temperature T of the soot particles, as shown in (4). Once T is known, the KL value can be calculated from Eq. (3).

$$\left[1-\left(\frac{e^{\left(C_2/\lambda_1 T\right)}-1}{e^{\left(C_2/\lambda_1 T_{a1}\right)}-1}\right)\right]^{\lambda_1^{\alpha_1}}=\left[1-\left(\frac{e^{\left(C_2/\lambda_2 T\right)}-1}{e^{\left(C_2/\lambda_2 T_{a2}\right)}-1}\right)\right]^{\lambda_2^{\alpha_2}} \tag{4}$$

Two high-speed cameras, Photron NOVA S9, were used in order to collect the radiation emitted by the soot within the flame at two specific wavelengths. For both cameras, the frame rate was set to 25,000 fps and a 100 mm f 2 Karl-Zeiss Makroplanar camera lens was used. One of the cameras was equipped with a narrowband interference filter with the transmission peak centred at 660 nm and 10 nm FWHM, while for the other a filter centred at 560 nm and 10 nm FWHM was utilized. A specific exposure time was set for each camera, due to the different intensity levels of radiation at each wavelength and each operating condition in order to make the most of the dynamic range of the camera.

In order to obtain KL evolution, a perfect matching (pixel by pixel) overlap between two images recorded by both cameras is needed. To achieve this, the use of different spatial correction tools is applied using MATLAB software. These tools take both images, one of them is spatially fixed and translation, rotation and scaling matrixes are applied in order to obtain a spatial transformation matrix to use in the other image. The left image in Fig. 7 shows the two raw images from both cameras (red and green colours) before applying the spatial transform matrix, while the right image shows the overlap after the use of the spatial transformation matrix where the perfect pixel matching is represented in yellow.

2.4. Image processing

For discussion in this study, an analysis of the average OH* radiation and KL collected from the 10 combustions cycles has been performed. For each recorded instant, OH* and KL data were averaged for the 10 combustion cycles to get matrices that represents the spatial distribution and average value of both species. These matrices were used later to calculate the temporal evolution of the in-cylinder average OH* chemiluminescence and KL. It is important to remark that for the CS2 analysis these average values were obtained using only the area corresponding to the radial lips (see the blue shadow from Fig. 4) while the whole piston area was considered for CS1. This approach provides a clear way to present an analysis of the temporal evolution of the combustion process for both pistons but requires integrating all the information within the cylinder in one value. Therefore, it would not provide spatial distribution information. For this reason, an additional approach was followed to present KL and OH* data with spatial and temporal resolution. Each of the KL and OH* matrices for each instant registered were divided into rings of different radius with 0.5 mm thickness and centred at the nozzle location, as shown in Fig. 8. For each ring, an average KL value was obtained according to Eq. (5). It was calculated with the ring area A_a and the sum of all pixels contained in the ring $KL_{cummul,a}$. Again, for CS1 the whole piston is considered while for CS2 only the region corresponding to the radial lips was taken into account (CS2-Lips). At each instant, the values obtained for the different rings are included in an array. Thus, all these arrays were later combined to build a matrix where the rows represented the different rings in which the images where divided (and the distance to the nozzle) while the columns represent the different instants registered.

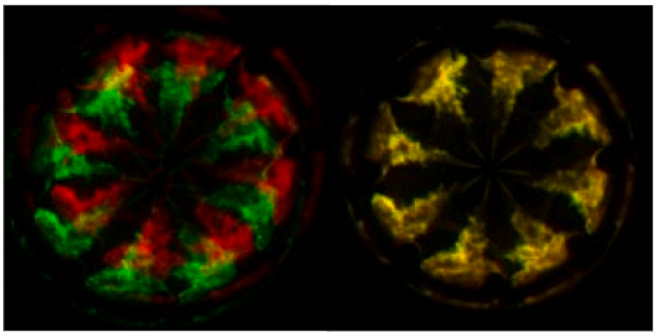

Fig. 7. 2-Colour pyrometry algorithm to obtain KL values. The left image corresponds to the image from both cameras (red and green colours), while the right image corresponds to the overlap image after the application of the spatial transform matrix (yellow colour).

$$KL_{mean}=KL_{cummul,a}/A_a \tag{5}$$

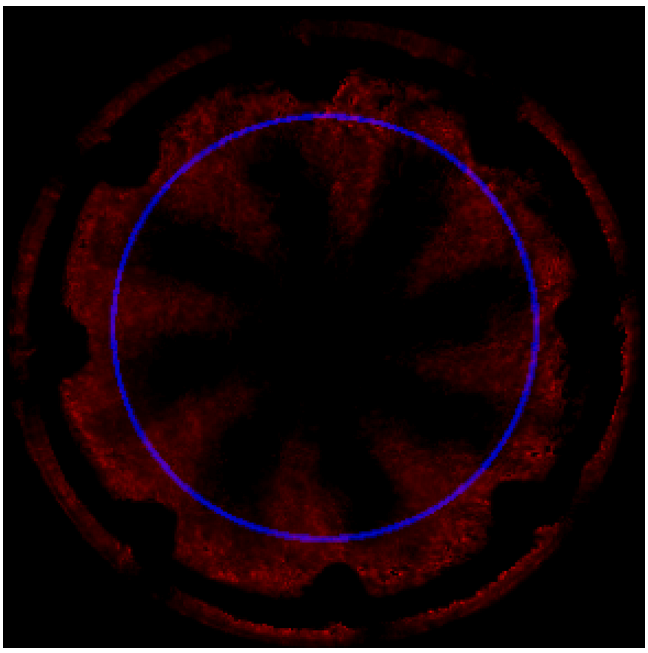

Fig. 8. Example of a ring (blue) to obtain the cumulative values of KL for CS1.

From now on, the graphic representation of these matrices will be identified as "radial maps". They represent the average KL value or OH* chemiluminescence of each ring at each registered instant, where the y-axis represents the radial distance to the nozzle while the x-axis represents the crank angle degree (CAD) after top dead centre (aTDC). In Fig. 9 an example of these radial maps can be observed.

To highlight the differences when comparing both pistons, relative difference radial maps were calculated for both KL and OH*. They were obtained by subtracting the information contained in the radial map of CS1 to CS2-Lips. Then, the resulting matrix is divided by the values of CS1 as per Eq. (6). Therefore, the positive values of the relative difference radial maps show a higher contribution from CS2-Lips, represented by green to a red in the colour pallet used, while the negative ones correspond to a higher contribution from CS1, represented by green to blue in the colour pallet. An example of these relative difference maps is shown in Fig. 10. It is important to highlight that the aim of these maps is not to quantify the parameter shown but to identify the region and time where differences between both pistons arise.

$$Relative\ radial\ map = \frac{(Map_{CS2Lips} - Map_{CS1})}{Map_{CS1}} \quad (6)$$

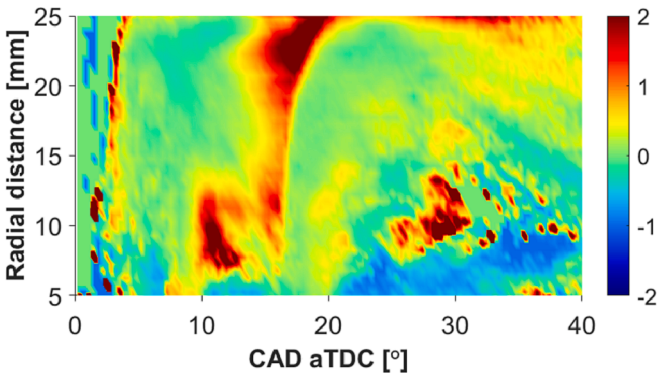

Fig. 10. Example of KL relative radial maps: Positive values (green to red colour) indicate a higher KL for CS2-Lips while negative values (green to blue) indicate a higher KL for CS1. The same discussion can be done for OH* relative radial maps.

3. Results and discussion

3.1. Baseline condition

The apparent Heat Release Rate (aHRR) obtained with CS1 and CS2 under baseline operating conditions is shown in Fig. 11. It is important to remark that this allows to compare both pistons, but it is not possible to isolate the effect of each side of the CS2. However, this data allows identifying if the combustion develops in the same way from a macroscopic point of view. The evolution of the aHRR from both pistons is similar, which indicates that the different bowl geometry does not have

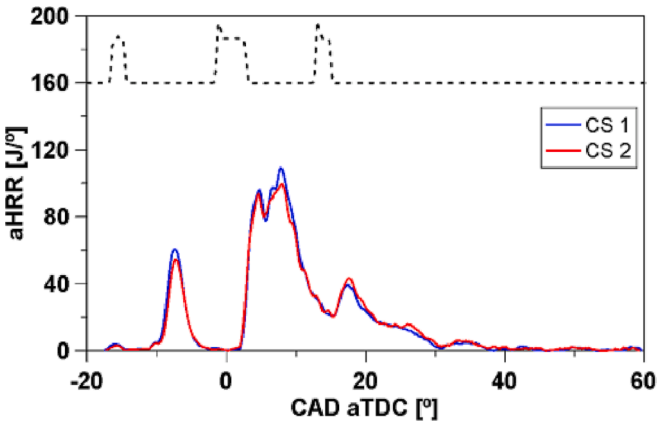

Fig. 11. Apparent Heat Release Rate (aHRR) at baseline operating condition using STD injector for both pistons. The blue line represents CS1 while the red line represents CS2. The injection strategy has been included in the upper part of the plot as a reference.

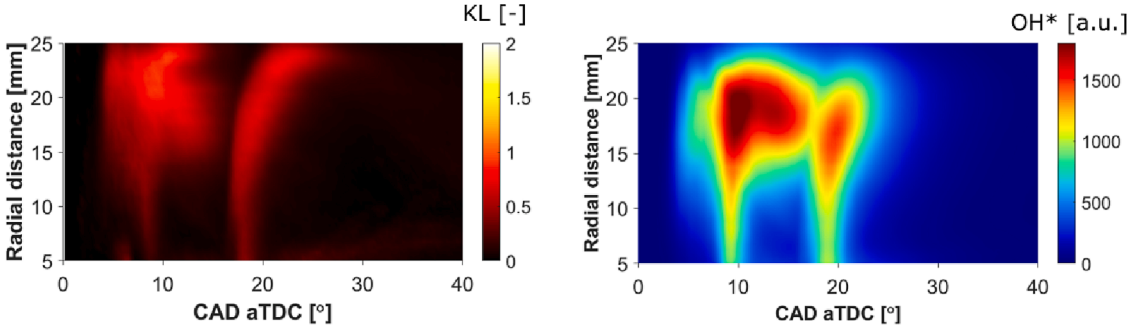

Fig. 9. Example of radial maps of KL values (left image) and OH* radiation (right image).

a significant impact on the combustion progress and energy released during the combustion process. This is consistent with the IMEP values obtained with CS1 and CS2: 6.8 bar and 6.7 bar, respectively.

Focusing on the soot evolution, in Fig. 12 the in-cylinder average KL is shown for both pistons under baseline operating conditions. In this case, as described in the methodology, the region with radial lips has been considered for CS2. When comparing both pistons, it is possible to see that less KL was measured for CS2-Lips (red line) compared with CS1 during the main-injection combustion event (from 3 to 18° aTDC). However, before the post-injection combustion event (around 18° aTDC), the KL values do not decrease with CS2-Lips as is observed with the other geometry, which indicates poorer oxidation of soot at this stage. This causes that at 20° aTDC the KL peak reached with the CS2-Lips to be close to the one measured with CS1. At the late stage of the combustion process (after 20° aTDC) no differences are observable between CS2-Lips and CS1.

To provide more insight into the soot evolution, radial maps for the CS2-Lips piston geometry are shown in Fig. 13, for KL (left) and OH* chemiluminescence (right). In addition, white arrows indicating the end of the main-injection (EOI_{Main}) and the start of post-injection (SOI_{Post}) were added at the top of both radial maps. At the first stages of combustion, KL appears between 12 mm and the bowl periphery. Then, it progresses towards the centre of the bowl until 10° aTDC. A first white arrow has been added to the radial map to highlight this movement. These instants correspond with the first soot peak observed in Fig. 12, which is related to the main-injection combustion event. Between the main and the post-injection combustion events (between 10° and 18° aTDC), the soot closer to the centre of the bowl (below 10 mm radius) seems to oxidize faster generating a retraction of the KL cloud towards positions far from the centre. This has been highlighted with a second white arrow on the KL map. The signal observed in the OH* chemiluminescence map during the same time interval and region, close to the bowl centre, confirms the appearance of oxidation reactions in this region of the bowl. They would be responsible for the retraction of the KL cloud between the main and post-injection combustion discussed before. This can be related to the fact that the flame is re-directed towards the piston centre has more oxygen available in this region, leading to leaner combustion than the one taking place at the periphery of the bowl. Besides, this behaviour is related to the decrease observed in the average KL curve (see Fig. 12) during the same stage of the combustion process. In contrast with this, above 12 mm, the OH* chemiluminescence also shows the existence of oxidation reactions which does not result in the complete disappearance of the related KL. It is expected that in this region the mixture is richer as the fuel trends accumulate there (despite the effect of the radial lips) and in that region there is not enough oxygen to oxidize all the soot formed. With the post-injection (after 18° aTDC), soot is observed close to the centre of the bowl and evolves towards the periphery of the piston. The high temperature inside the combustion chamber allows the fuel to ignite fast resulting in a short lift-off length while the post-injection event lasts. After this, the oxidation of the soot is faster close to the centre and the soot remaining is located closer to the periphery of the bowl.

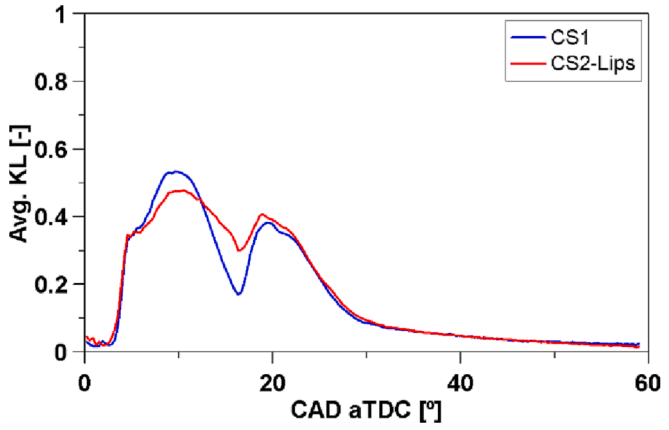

Fig. 12. Average KL evolution curves for CS1 (blue line) and CS2-Lips (red line).

The differences related between CS1 and CS2-Lips can be analysed thanks to the relative radial maps for both KL (left) and OH* chemiluminescence (right) presented in Fig. 14. During the main-injection combustion event, a higher soot cloud close to the centre of the bowl is observed for CS2-Lips indicating that this geometry displaces more soot to the centre of the bowl compared to CS1. Between the main and post-injection combustion, a higher soot cloud is observed for the whole piston using CS2-Lips which is consistent with the higher KL values discussed in Fig. 12. Furthermore, during the post-injection combustion event (after 20° aTDC), a higher KL cloud remains at the bowl periphery for CS2-Lips and the oxidation reactions observed in OH* images (right) are not sufficient to oxidize it. The result suggest that this geometry has difficulties to oxidize soot in this zone compared to CS1, which can be related with the fact CS2-Lips accumulates a richer mixture in this region, as already discussed in Fig. 13. At the late stages of combustion, some differences can be still observed between both pistons. From 25° to 30° aTDC, the CS2-Lips present higher values of KL bellow 15 mm radius. However, after 30° the soot at this region increases for CS1. This can be caused by the different movement promoted by each geometry. As suggested previously, CS2-Lips allows the flame to reach regions closer to the nozzle faster than with CS1. Besides, this gives some time for the first geometry for additional oxidation with the oxygen still available there. Therefore, that soot cloud in CS2-Lips reaches the centre of the piston before and has some time to oxidize and decrease before a similar displacement is completed with the CS1.

3.2. Geometry performance under EGR operating conditions

In this study, the performance of CS1 and CS2 have also been evaluated for 18% and 15% of O_2 (in volume) concentration. In this way, the behaviour of the piston under more unfavourable oxidation conditions can be evaluated. In Fig. 15, the aHRR for 21% (green), 18% (red) and 15% (blue) O_2 concentration for CS1 (solid line) and CS2 (dashed line) is shown. At 18% O_2, less energy was obtained for CS2 during the second pilot injection combustion event (around −3° aTDC). Then, during the main injection combustion event, a slightly higher and delayed main combustion peak is obtained for CS2. This suggests a more premixed combustion, caused by the lower energy released during the previous phase. When looking at 15% O_2, almost no differences can be observed between both pistons.

In addition, the IMEP values obtained for all these tests have been summarized in Table 4 where, despite the difference mentioned, a similar performance was obtained with both pistons for the two additional operating conditions.

The average KL curves obtained for the three different oxygen concentration cases and the two geometries are shown in Fig. 16. The decrease of oxygen provides a clear KL increasing trend (for both pistons) as expected. With 18% O_2 (red), as similar behaviour of CS2-Lips with reference to CS1 as with the baseline case is observed. Less soot is formed during the main injection event while a shy soot reduction is obtained between the main and post-injection combustion. However, the oxygen reduction harms the CS1 geometry during this stage and the difference with CS2-Lips is clearly reduced. Continuing with the process, no differences are observed between the geometries during the post-injection combustion (between 18° and 30° aTDC). At the late stages of combustion (after 30° aTDC), higher KL values are reported for CS2-Lips, indicating a better late oxidation with CS1. Nevertheless, this was not observed with 21% O_2. With 15% O_2 (blue), a clear KL reduction is achieved with CS2-Lips compared to the other geometry along the whole combustion process. In this condition, more soot is formed as shown by the higher KL values reached. Besides, oxidation is slower as it is

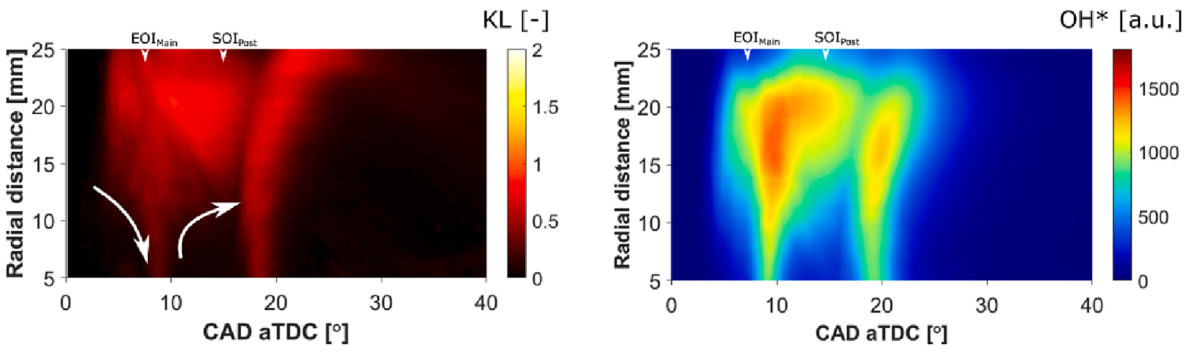

Fig. 13. KL factor (left) and OH* chemiluminescence (right) radial maps for CS2-Lips.

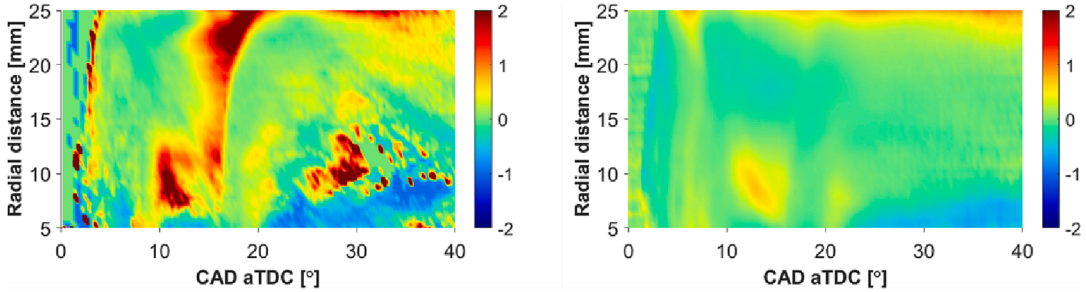

Fig. 14. KL factor (left) and OH* (right) relative radial maps comparing CS2-Lips and CS1. Positive values (green to red colour) indicate higher values for CS2-Lips while negative values (green to blue colour) indicate higher values for CS1.

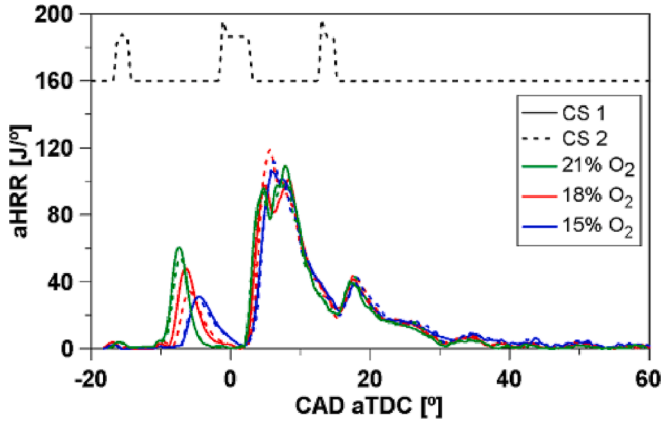

Fig. 15. Apparent Heat Release Rate at 21% (green), 18% (red) and 15% (blue) O_2 using STD injector for both pistons. The solid line represents CS1 and the dashed line represents CS2. The injection strategy has been included in the upper part of the plot as a reference.

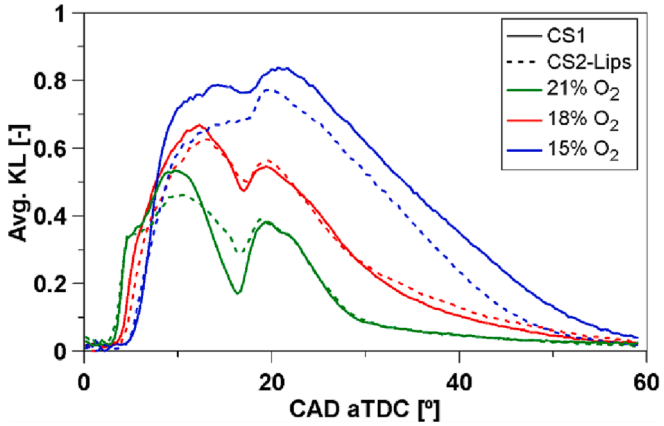

Fig. 16. Average KL evolution at 21% (green), 18% (red) and 15% (blue) O_2 for both pistons: CS1 (solid-line) and CS2-Lips (dashed-line).

Table 4
IMEP at different O_2 concentration test conditions.

Piston	%O_2 (vol.)	IMEP (bar)
CS1	18/15	6.9/6.7
CS2	18/15	6.7/6.6

suggested by the absence of a gap in the KL curve between the main and post-injection combustion events in contrast with higher oxygen concentration operating conditions. In this scenario, KL values achieved by CS1 are much higher than those of CS2-Lips which suggest a higher improvement in comparison with CS1 than that observed with more oxygen availability. This suggests that the radial lips of the CS2 form less soot at high EGR conditions, indicating a better use of oxygen inside the combustion chamber. After 25° aTDC, the KL reduction velocity is equivalent for both geometries, which indicates that the late oxidation process is similar with both geometries. This is coherent with the fact that no clear dependences between the geometry and the late oxidation was identified in any of the other operating conditions analysed.

The radial maps of KL and OH* chemiluminescence presented in Fig. 17 allows to identify the differences between 18% and 15% O_2. In terms of KL distribution, the decrease observed at baseline condition between the main and the post-injection combustion events is not visible for the other oxygen concentration conditions, especially for 15% O_2. This is consistent with the average KL evolution shown in Fig. 16. At the late stages of combustion, the 15% O_2 case shows KL values between 10 mm radius and the periphery of the bowl, indicating a much larger area where soot remains in comparison with the other two cases with higher oxygen content. The OH* chemiluminescence decreases with the oxygen

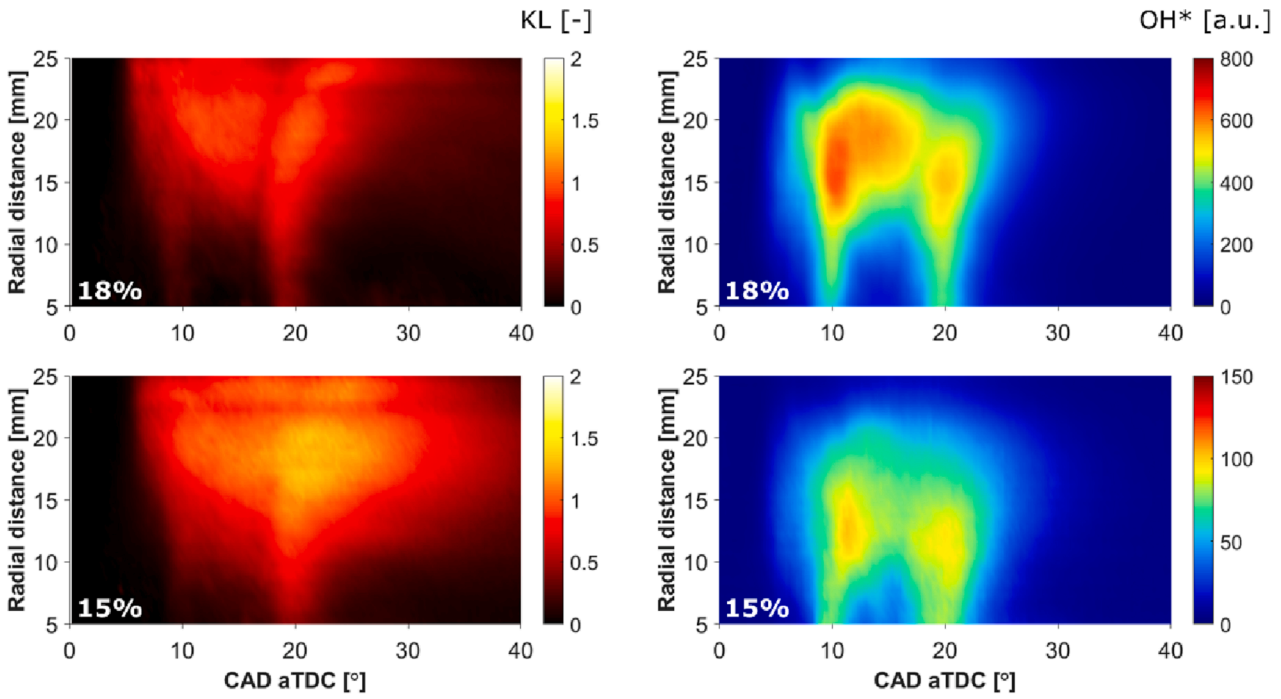

Fig. 17. KL factor (left) and OH* chemiluminescence (right) radial maps for CS2-Lips at 18% (top) and 15% (bottom) O_2 conditions.

content, due to the lower oxygen availability to oxidize hydrocarbons and soot during the combustion process. Therefore, the scale from OH* maps was reduced by almost an order of magnitude for each concentration evaluated. Additionally, the spatial distribution of the OH* signal moves from the bowl periphery to the centre of the piston as the oxygen concentration is decreased. This could be related to the fact that a much richer mixture is achieved close to the periphery of the bowl, reducing the reactivity in this region. In the case of 21% O_2, the maximum distance where the oxidation activity appears is around 25 mm of radial distance while for 18% and 15% of O_2 is 23 mm and 20 mm, respectively. For this reason, the soot that remains at the periphery of the bowl is not oxidized and this fact could explain the weaker oxidation reported in Fig. 16.

Relative radial maps between CS1 and CS2-Lips are shown in Fig. 18. At 18% O_2, slight differences between pistons are reported, especially when compared with the baseline condition. In this case, CS1 and CS2-Lips are quite similar between the main and post-injection combustion events as no blue or red regions are visible. This is consistent with the gap reduction in KL curves reported in Fig. 16. In addition, during the late combustion stage (after 25° aTDC) a higher KL cloud for CS2-Lips between 7 mm and 20 mm radius is detected. This is consistent with the higher values in KL curves (red dashed line) reported in Fig. 16 for this piston. However, this has not been observed in any of the other operating conditions tested and has not been successfully related with the effect of the different geometry. Furthermore, the difference is even lower than the variability of the measurement at that stage of the

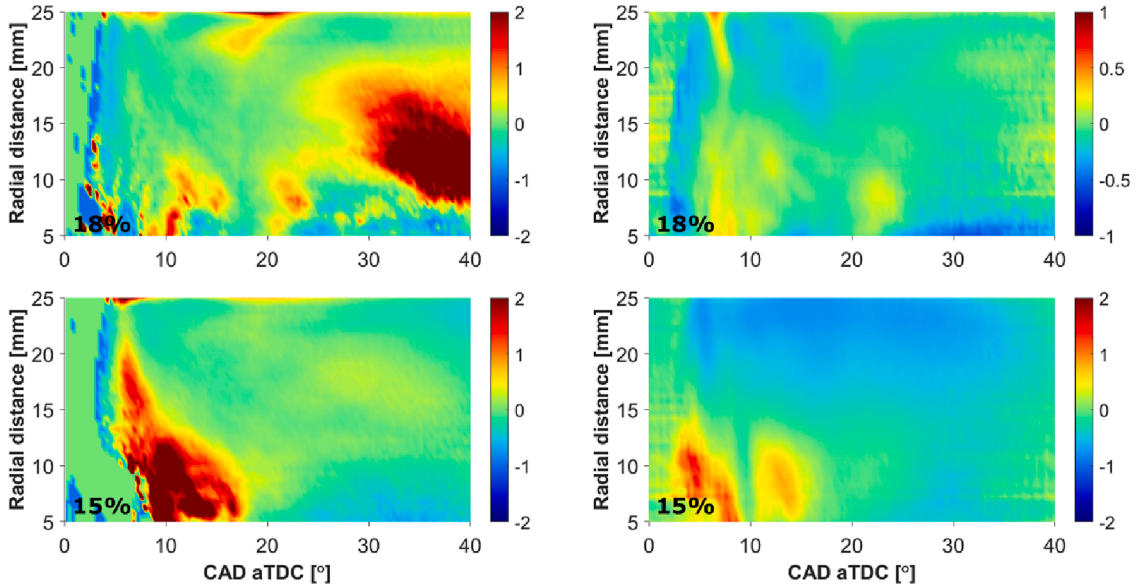

Fig. 18. KL factor (left) and OH* (right) relative radial maps at 18% (top) and 15% (bottom) O_2 conditions. Positive values (green to red colour) indicate higher values for CS2-Lips while negative values (green to blue colour) indicate higher values for CS1.

combustion process and, therefore, it is not conclusive.

Remarkable differences are obtained at the lowest oxygen concentration condition compared with others reported in this study. At 15% O_2, a higher KL cloud is detected for CS2-Lips bellow 20 mm radius during the main-injection combustion event and evolves towards the centre of the bowl until the start of the post-injection combustion. This is represented by the red cloud visible in the relative difference radial map. This behaviour confirms that CS2-Lips displaces a higher soot quantity toward the bowl centre compared to CS1. However, according to results presented in Fig. 16, considering the whole region KL values are lower than those of CS1. The higher oxidation activity (OH* signal) provided by CS2-Lips in this region and the later disappearance of KL confirms the capability of this geometry to improve oxygen usage close to the bowl centre and the benefits of using it under very low oxygen concentration. After 20° the combustion process and soot formation evolve in a similar way for both pistons. However, the KL spatial distribution is different. While with CS1 it is mainly located at the periphery of the bowl with CS2-Lips it can be found between 10 and 20 mm.

3.3. CDS injector and radial-lip design interaction

When using the same injection strategy for the STD and the CDS injectors, their different geometry leads to a different amount of fuel injected which, at the end, results in a higher IMEP for the second one. For this reason, the main-injection electric pulse was reduced 90 μs for the CDS injector to maintain the same IMEP as the reference for comparison between both injectors. However, the dwell time between the main and post-injection was kept constant to not increase the time available for soot oxidation between both events, as it was observed that it was a critical process when comparing CS1 and CS2-Lips. At baseline condition (21% O_2), the use of CDS injector has certain influence on the combustion behaviour in comparison with STD injector. An earlier decrease of aHRR corresponding to the main injection combustion can be seen in Fig. 19. Although the injection duration is slightly shorter for the CDS injector, it cannot explain the difference observed. Therefore, other effects related to the CDS concept like better atomization and air–fuel mixture are being effective. The post-injection combustion event is slightly advanced for the same reason. Despite this, the same IMEP was reached with both injectors, as reported in Table 5.

In Fig. 20, average KL evolution curves are reported using CDS injector at baseline conditions. These results are compared with the previous ones where the STD injector was used. For both combustion systems (CS1 and CS2-Lips), no differences can be appreciated during the main-injection combustion between the CDS and STD injectors. When the soot formation slows down (peak of the curve) and the soot oxidation starts to dominate the soot evolution, a different trend is

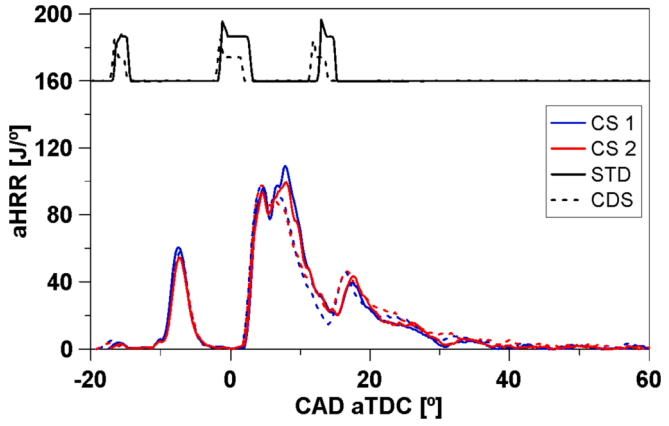

Fig. 19. Apparent Heat Release Rate at baseline condition using STD (solid-line) and CDS (dashed-line) injectors for CS1 (blue line) and CS2 (red line). The injection strategy has been included in the upper part of the plot as a reference.

Table 5
IMEP at the nominal condition for STD and CDS injectors.

Piston	Injector	%O_2 (vol.)	IMEP (bar)
CS1	STD	21	6.8
	CDS		6.7
CS2	STD	21	6.7
	CDS		6.7

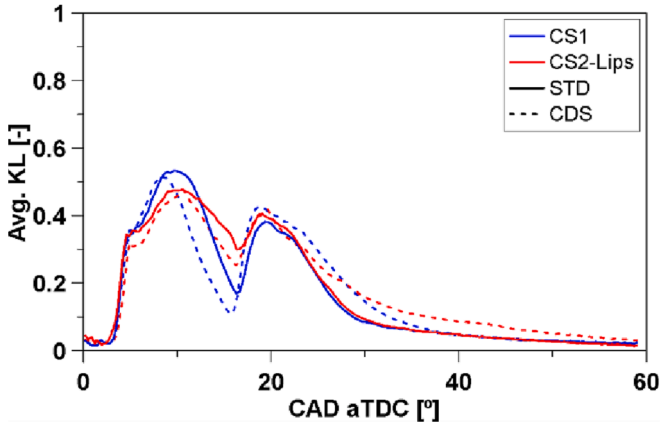

Fig. 20. Average KL evolution at nominal condition using STD (solid line) and CDS (dashed line) injectors for CS1 (blue line) and CS2-Lips (red line).

observed for the CDS injector, regardless of the piston used. The KL values decrease earlier with CDS, achieving lower values when compared to the STD (minimum KL). In addition, for CS1 and CS2-Lips, the CDS seems to be also promoting faster soot oxidation since the curve slope is steeper. In this way, the combination of CDS and radial lips is providing not only lower maximum KL values but also earlier and faster soot oxidation during the main combustion event. This is coherent with the aHRR curves discussed previously, evidencing that the CDS is favouring the mixing process. Moving forward, an opposite trend can be observed when the post-injection occurs. The CDS injector starts the post-injection combustion from lower KL values than STD but it reaches slightly higher values when the curve achieves the maximum KL. In addition, the oxidation phase of the post-injection combustion is also slowed down when using the CDS, a behaviour that is completely different when compared with the main combustion. This is mainly explained by the reason that the post-injection duration was kept the same for both injectors, not being corrected for the CDS as was done during the main injection. It means that more fuel mass is injected with this hardware during the post-injection, promoting higher soot formation in this phase. As this extra soot mass is formed at the moment that in-cylinder pressure and temperature are decreasing (late combustion phase), its oxidation process is also more difficult and slower. This is also observed in the aHRR, which at the late stages show slightly higher values than those of STD which correspond with a longer oxidation activity.

4. Conclusions

The current study aimed to analyse two pistons with different radial-lip geometries, trying to identify the differences in terms of the combustion process and soot formation by employing an optical engine based on a compression ignition engine. High-soot conditions with low-oxygen concentration were applied for evaluating the potential of these piston geometries to reduce soot formation and oxidize it when operating under these critical engine conditions. Furthermore, the use of two different injector systems was done to study the combined effect. To achieve this, in-cylinder soot formation was analysed through the 2C-

pyrometry KL factor and high-speed OH* chemiluminescence images as a tracer of the oxidation reactions inside the piston. The main results are summarized below:

- The results showed that both combustion systems tested (CS1 and CS2-Lips) are capable to promote the movement of the flame from the periphery towards the bowl centre, allowing the flame to achieve regions where fresh oxygen is available. However, the analysis confirmed The C2-Lips, which has a more pronounced radial lip profile, drives the flames closer to the bowl centre than the CS1 design. This factor not only makes the oxidation process faster but also reduces the soot formation.
- At baseline conditions (21% O_2), clear differences were observed during the main injection combustion and before the post-injection combustion at baseline conditions. CS2-Lips forms less soot than CS1 during the main-injection combustion. However, the oxidation between main and post-injection combustion is poorer for this geometry. After the post-injection combustion event, no differences arise between these two pistons indicating that the geometry of the radial lips does not seem to affect the late oxidation process.
- When increasing EGR ratio, from 21% O_2 (no-EGR) to 15% O_2, the differences between CS1 and CS2-Lips are more prominent. The CS2-Lips proved to work better than CS1 under very low oxygen concentration (15% O_2), providing much lower soot formation.
- Regarding the injector nozzles, certain differences were observed between CDS and STD injectors in terms of combustion behaviour. The aHRR showed a faster combustion during the main injection for the CDS with respect to the STD. This had an impact on soot formation and oxidation, similar with both piston geometries. Besides, at the late stages of combustion, the injection strategy used lead to longer combustion and slower final oxidation for both pistons. Therefore, a relation between the CDS injector and the radial-lip design was not identified.

In summary, the effectiveness of the radial-lip concept was confirmed by the results obtained under different engine conditions. The more pronounced lips provide an improvement of the recirculation effect as well as the reduction of the flame-to-flame interaction while promoting the use of in-cylinder oxygen. However, its effect on soot formation was more appreciable at operating conditions under low oxygen scenarios, higher loads or during the main injection combustion event, where the need of oxygen is higher.

CRediT authorship contribution statement

José V. Pastor: Conceptualization, Project administration, Resources. **Carlos Micó:** Supervision, Methodology, Writing – review & editing. **Felipe Lewiski:** Writing – review & editing, Formal analysis, Data curation. **Francisco J. Tejada:** Software, Writing – original draft, Investigation, Data curation. **Alberto Vassallo:** Conceptualization, Supervision. **Francesco C. Pesce:** Supervision, Visualization. **Giacomo Belgiorno:** Investigation, Writing – review & editing.

Declaration of Competing Interest

The authors declare that they have no known competing financial interests or personal relationships that could have appeared to influence the work reported in this paper.

Data availability

The authors do not have permission to share data.

References

[1] EEA, European Environment Agency n.d. https://www.eea.europa.eu/themes/air (accessed December 13, 2022).
[2] Introducing Soot-free Transport - International Council on Clean Transportation n. d. https://theicct.org/introducing-soot-free-transport/ (accessed August 22, 2022).
[3] García A, Monsalve-Serrano J, Rückert Roso V, Santos Martins ME. Evaluating the emissions and performance of two dual-mode RCCI combustion strategies under the World Harmonized Vehicle Cycle (WHVC). Energ Conver Manage 2017;149: 263–74. https://doi.org/10.1016/J.ENCONMAN.2017.07.034.
[4] Benajes J, García A, Monsalve-Serrano J, Lago SR. Fuel consumption and engine-out emissions estimations of a light-duty engine running in dual-mode RCCI/CDC with different fuels and driving cycles. Energy 2018;157:19–30. https://doi.org/10.1016/J.ENERGY.2018.05.144.
[5] Benajes J, García A, Monsalve-Serrano J, Boronat V. Dual-Fuel Combustion for Future Clean and Efficient Compression Ignition Engines. Appl Sci 2017;7:1–16. https://doi.org/10.3390/APP7010036.
[6] Benajes J, García A, Monsalve-Serrano J, Balloul I, Pradel G. Evaluating the reactivity controlled compression ignition operating range limits in a high-compression ratio medium-duty diesel engine fueled with biodiesel and ethanol. Int J Engine Res 2017;18:66–80. https://doi.org/10.1177/1468087416678500.
[7] Pastor JV, Garcia-Oliver JM, Micó C, Tejada FJ. Comparison of the Diffusive Flame Structure for Dodecane and OMEX Fuels for Conditions of Spray A of the ECN. SAE Tech Pap 2021;3(1):402–11.
[8] Pastor JV, Garcia-Oliver JM, Micó C, Tejada FJ. Combustion Behaviour of Blends of Synthetic Fuels in an Optical Single Cylinder Engine. SAE Tech Pap 2021. https://doi.org/10.4271/2021-24-0038.
[9] Pastor JV, García A, Micó C, Lewiski F. Soot reduction for cleaner Compression Ignition Engines through innovative bowl templates. Int J Engine Res 2021;22: 2477–91. https://doi.org/10.1177/1468087420951324.
[10] Pastor JV, García A, Micó C, Lewiski F, Vassallo A, Pesce FC. Effect of a novel piston geometry on the combustion process of a light-duty compression ignition engine: An optical analysis. Energy 2021;221:119764. https://doi.org/10.1016/j.energy.2021.119764.
[11] Rao L, Zhang Y, Kim D, Su HC, Kook S, Kim KS, et al. Effect of after injections on late cycle soot oxidation in a small-bore diesel engine. Combust Flame 2018;191: 513–26.
[12] Eismark J, Andersson M, Christensen M, Karlsson A, Denbratt I. Role of Piston Bowl Shape to Enhance Late-Cycle Soot Oxidation in Low-Swirl Diesel Combustion. SAE Int J Engines 2019;12:233–49. https://doi.org/10.4271/03-12-03-0017.
[13] Neely GD, Sasaki S, Sono H. Investigation of alternative combustion crossing stoichiometric air fuel ratio for clean diesels. SAE Tech Pap 2007. https://doi.org/10.4271/2007-01-1840.
[14] Smith A. Ricardo low emissions combustion technology helps JCB create the off-highway industry's cleanest engine. Ricardo Press Release 2010:4–6.
[15] Busch S, Zha K, Kurtz E, Warey A, Peterson R. Experimental and Numerical Studies of Bowl Geometry Impacts on Thermal Efficiency in a Light-Duty Diesel Engine. SAE Tech Pap 2018;2018. https://doi.org/10.4271/2018-01-0228.
[16] Dahlstrom J, Andersson O, Tuner M, Persson H. Experimental Comparison of Heat Losses in Stepped-Bowl and Re-Entrant Combustion Chambers in a Light Duty Diesel Engine. SAE Tech Pap 2016. https://doi.org/10.4271/2016-01-0732.
[17] Di Blasio G, Ianniello R, Beatrice C, Pesce FC, Vassallo A, Belgiorno G. Experimental Investigation on an Innovative Additive Manufacturing-Enabled Diesel Piston Design to improve Engine-out Emissions and Thermal Efficiency beyond Euro6. THIESEL 2020 Conference on Thermo- and Fluid Dynamic Processes in Direct Injection Engines, n.d.
[18] Eismark J, Christensen M, Andersson M, Karlsson A, Denbratt I. Role of fuel properties and piston shape in influencing soot oxidation in heavy-duty low swirl diesel engine combustion. Fuel 2019;254:115568. https://doi.org/10.1016/J.FUEL.2019.05.151.
[19] Belgiorno G, Boscolo A, Dileo G, Numidi F, Pesce FC, Vassallo A, et al. Experimental study of additive-manufacturing-enabled innovative diesel combustion bowl features for achieving ultra-low emissions and high efficiency. SAE Tech Pap 2021;3(1):672–84.
[20] Millo F, Piano A, Roggio S, Bianco A, Pesce FC, Vassallo AL. Numerical Assessment of Additive Manufacturing-Enabled Innovative Piston Bowl Design for a Light-Duty Diesel Engine Achieving Ultra-Low Engine-Out Soot Emissions. SAE Int J Engines 2021;15:3–15. https://doi.org/10.4271/03-15-03-0022.
[21] Millo F, Piano A, Roggio S, Pastor JV, Micó C, Lewiski F, et al. Mixture formation and combustion process analysis of an innovative diesel piston bowl design through the synergetic application of numerical and optical techniques. Fuel 2022; 309:122144.
[22] Payri R, De La Morena J, Monsalve-Serrano J, Pesce FC, Vassallo A. Impact of counter-bore nozzle on the combustion process and exhaust emissions for light-duty diesel engine application. Int J Engine Res 2018;20:46–57. https://doi.org/10.1177/1468087418819250.
[23] Payri R, Hardy G, Gimeno J, Bautista A. Analysis of counterbore effect in five diesel common rail injectors. Exp Therm Fluid Sci 2019;107:69–78. https://doi.org/10.1016/J.EXPTHERMFLUSCI.2019.05.008.
[24] Heywood J. Internal combustion engine fundamentals. vol. 26. Second. 1988. doi: 10.5860/choice.26-0943.
[25] Serizawa K, Ueda D, Mikami N, Tomida Y, Weber J. Realizing Robust Combustion with High Response Diesel Injector with Controlled Diffusive Spray Nozzle and Closed Loop Injection Control. SAE Tech Pap 2017:2017-March. https://doi.org/10.4271/2017-01-0845.

[26] Tu PW, Xu H, Srivastava DK, Dean K, Jing D, Cao L, et al. Numerical Investigation of GDI Injector Nozzle Geometry on Spray Characteristics. SAE Tech Pap 2015: 2015-Septe. https://doi.org/10.4271/2015-01-1906.
[27] Higgins B, Siebers DL. Measurement of the Flame Lift-Off Location on DI Diesel Sprays Using OH Chemiluminescence. SAE Tech Pap 2001. https://doi.org/10.4271/2001-01-0918.
[28] Matsui Y, Kamimoto T, Transactions SM-S, 1979 U. A study on the time and space resolved measurement of flame temperature and soot concentration in a DI diesel engine by the two-color method. SAE Technical Papers 1979. doi: 10.4271/790491.
[29] Zhao H, Ladommatos N. Optical diagnostics for soot and temperature measurement in diesel engines. Prog Energy Combust Sci 1998;24:221–55. https://doi.org/10.1016/S0360-1285(97)00033-6.